Gating of *Shaker* K^+ Channels: I. Ionic and Gating Currents

Enrico Stefani,* Ligia Toro,* Eduardo Perozo,‡§ and Francisco Bezanilla‡

*Department of Molecular Physiology and Biophysics, Baylor College of Medicine, Houston, Texas 77030, and ‡Department of Physiology, University of California at Los Angeles, Los Angeles, California 90024 USA

ABSTRACT Ionic and gating currents from noninactivating *Shaker* B K^+ channels were studied with the cut-open oocyte voltage clamp technique and compared with the macropatch clamp technique. The performance of the cut-open oocyte voltage clamp technique was evaluated from the electrical properties of the clamped upper domus membrane, K^+ tail current measurements, and the time course of K^+ currents after partial blockade. It was concluded that membrane currents less than 20 μA were spatially clamped with a time resolution of at least 50 μs. Subtracted, unsubtracted gating currents with the cut-open oocyte voltage clamp technique and gating currents recorded in cell attached macropatches had similar properties and time course, and the charge movement properties directly obtained from capacity measurements agreed with measurements of charge movement from subtracted records. An accurate estimate of the normalized open probability $P_O(V)$ was obtained from tail current measurements as a function of the prepulse V in high external K^+. The $P_O(V)$ was zero at potentials more negative than −40 mV and increased sharply at this potential, then increased continuously until −20 mV, and finally slowly increased with voltages more positive than 0 mV. Deactivation tail currents decayed with two time constants and external potassium slowed down the faster component without affecting the slower component that is probably associated with the return between two of the closed states near the open state. In correlating gating currents and channel opening, Cole-Moore type experiments showed that charge moving in the negative region of voltage (−100 to −40 mV) is involved in the delay of the conductance activation but not in channel opening. The charge moving in the more positive voltage range (−40 to −10 mV) has a similar voltage dependence to the open probability of the channel, but it does not show the gradual increase with voltage seen in the $P_O(V)$.

INTRODUCTION

Voltage-dependent ion channels are integral membrane proteins that respond to changes in membrane potential with rapid variations in membrane permeability to ions. The sequence of events leading to the opening of ion channel pores is thought to require the movement of charged elements that sense the membrane electric field. The electrical manifestations of the movement of these charged elements are the gating currents (Armstrong and Bezanilla, 1973; Schneider and Chandler, 1973; Bezanilla, 1985). Ionic current measurements mainly reflect the channel open state, while gating currents give additional information on the channel transitions occurring among many closed states prior to channel opening. Thus ionic currents in conjunction with gating current measurements may provide an insight on the molecular basis of the different conformations of the channel protein during voltage activation.

Ionic and gating currents from expressed K^+ channels in *Xenopus* oocytes using the cut-open oocyte vaseline gap technique (COVG) have been recently recorded (Bezanilla et al., 1991; Perozo et al., 1992). In these reports, gating currents were isolated by the established procedure of subtracting membrane linear capacity and resistive components from the stimulating pulse with membrane currents elicited by small negative pulses (P/-4) (Bezanilla and Armstrong, 1977; Bezanilla, 1985). The properties of these subtracted gating currents were later confirmed in the initial recordings of unsubtracted gating currents (Taglialatela and Stefani, 1993; Perozo et al., 1993). In this work we further evaluate ionic and gating current properties in *Shaker* K^+ channels after maximizing their expression channels and improving the performance of the COVG technique. In addition, we compared charge movement properties with the COVG and macropatch techniques. The measurements were performed in normal conducting K^+ channels and in a pore mutant that prevented K^+ conduction without affecting gating current properties (Perozo et al., 1993). In this first paper, after discussing the time resolution and spatial homogeneity of the COVG technique we studied in detail K^+ ionic and gating current properties which are the basis for the model of ion channel activation discussed in the second paper (Bezanilla et al., 1994).

MATERIALS AND METHODS

Oocyte preparation and injection of mRNAs

Xenopus laevis oocytes (stage V–VI) were used. One day before injection of cRNA, oocytes were treated with collagenase (200 units/ml, GIBCO) in a Ca^{2+}-free solution, to remove the follicular layer. Oocytes were microinjected with 40–60 nl of cRNA at ~1 μg/μl (40–60 ng) and maintained at 19°C in an amphibian saline solution supplemented with 50 μg/ml gentamycin and 2.5 mM pyruvate, for 2–6 days. All the recordings reported were performed at room temperature (22°C), 2–7 days after cRNA injection.

cRNA preparation

cDNA encoding *Shaker* H4 K^+ channel, which is nearly identical to the *Shaker*B clone, was used (Kamb et al., 1988; Tempel et al., 1987). The

Received for publication 19 August 1993 and in final form 10 December 1993.

Address reprint requests to Francisco Bezanilla, Department of Physiology, UCLA School of Medicine, 405 Hilgard Ave., Los Angeles, CA 90024.

§Present address: Centro de Biofisica y Bioquimica, IVIC, Apartado 21827, Caracas 1020A, Venezuela.

0006-3495/94/04/996/15 $2.00

following clones were used: *Shaker* H4 (*Sh*H4), *Shaker* H4 with inactivation removed which has the deletion D6–46 (*Sh*H4-IR) (Hoshi et al., 1990), and the corresponding nonconducting counterpart *Sh*H4-IR-W434F (Perozo et al., 1993). To increase the external tetraethylammonium (TEA) sensitivity we used the T449Y mutation in the *Sh*H4-IR construct (*Sh*H4-IR-T449Y) (MacKinnon and Yellen, 1990). We have determined conditions for the synthesis of cRNA, which have allowed us to record reliably and consistently large ionic and gating currents. We examined several ratios of capping nucleotide (GpppG)/GTP (i.e., 0.6/0.2, 0.6/1.0, and 1/0.4 mM). We found that a ratio of 0.6/1 mM was optimal and that GpppG had to be dissolved in Tris-EDTA (TE) buffer. cDNA was transcribed using T7 RNA polymerase in the presence of 1 mM NTP, 0.6 mM GpppG (Pharmacia, Piscataway, NJ) and 0.5 unit/μl of Inhibit-ACE RNase inhibitor (5Prime→ 3Prime, Boulder, CO). Another factor to increase expression in the oocytes is to alter the nature of the 5′-untranslated leader of the cRNA (Fu et al., 1991). A construct of the *Sh*H4-IR K^+ channel made by Dr. MacKinnon (Department of Neurobiology, Harvard Medical School), in which bases 1–223 of the original 5′-untranslated leader were deleted, gives large expression.

Solutions

Solutions were made by mixing stock isotonic solutions of the main cation (220 mOsm) containing 10 mM 4-(2-hydroxyethyl)-1-piperazineethanesulfonic acid (HEPES) at pH 7.0. The abbreviations are: GLU, glutamate; MES, methanesulfonate; NMG, *n*-methylglucamine; and TEA. The stock isotonic solutions were: NaCl, KCl, NaMES, KMES, K-GLU, TEA-MES, NMG-MES, NMG-GLU, and TEA-GLU 110 mM, and $Ca(MES)_2$ 74 mM. EGTA (1 mM) was added to solutions for intracellular perfusion. A typical solution for recording gating currents was made by mixing NaMES and $Ca(MES)_2$ to obtain NaMES 107 mM, $Ca(MES)_2$ 2 mM, HEPES 10 mM; its abbreviation would be NaMESCa2. Standard solutions for intracellular micropipettes were 3 M KCl and 3 M NaMES, 10 mM NaCl, and 1 mM Na_2EGTA buffered to pH 7.0 with 10 mM HEPES. Bath solutions were replaced in the top and guard compartments. The solution replacement in the top chamber can be achieved in seconds by a perfusion system (ca. 1 ml/s) and at a slower rate in the guard compartment.

Macropatch technique

To perform cell-attached macropatches, the oocytes' viteline membrane was removed manually after incubation in a hyperosmotic solution (NaMESCa2 + 300 mM sucrose) (Methfessel et al., 1986). In all the macropatch experiments the bath solution was KMESCa2 with 1 mM Na_2EGTA that brings the oocyte membrane potential close to 0 mV. Gating and ionic currents were recorded with an Axopatch 200A patch amplifier (Axon Instruments, Inc., Burlingame, CA).

Data acquisition

An IBM compatible personal computer was used for data acquisition. Analog signals were filtered at one-fourth the sampling frequency. The oocyte membrane potential was generally clamped to a holding potential (HP) of −90 mV. Linear capacity and resistive components were digitally subtracted by scaled control currents obtained with small negative (P/-4) or positive pulses (P/4) of 1/4th the test pulse amplitude from negative (−120 to −150 mV) or positive (20 mV) subtracting holding potentials (SHP), respectively. The adequacy of our subtracting protocol was tested by using different SHP and comparing subtracted and unsubtracted gating current records.

Schematic diagram of the COVG amplifier

Experiments were performed with the COVG technique (Taglialatela et al., 1992) and with the conventional patch clamp technique. The COVG technique is a low noise fast clamp that allows control of the internal solution. Fig. 1 is a scheme of a recent upgrade to achieve even a higher clamp speed and lower noise. The main changes to the system were: 1) active clamps were set for the top and guard chambers, 2) control amplifiers did not have negative feedback components other than the electrodes and the preparation (open loop gain), and 3) the voltage signal was directly fed from the *V1* microelectrode to the negative input of the control amplifier A4.

The oocyte was placed in a triple compartment perspex, with a diameter of 700 μm for the top and bottom rings. The circuit consists of three active clamps; amplifier A4 maintains the oocyte interior at ground as measured by the intracellular microelectrode tip V1, and amplifiers A5 and A6 clamp to the command pulse the top and the guard chambers, respectively. The membrane potential is differentially recorded between V1 and V2. The microelectrodes had resistances of about 1 MΩ which set a time constant near 1 μs in the voltage-recording system with 1 pF as the input capacity of A1. Electrodes P1 (*top chamber*) and GS1 (*guard shield*) are sensing electrodes, and P2 and GS2 deliver the current to maintain P1 and GS2 at

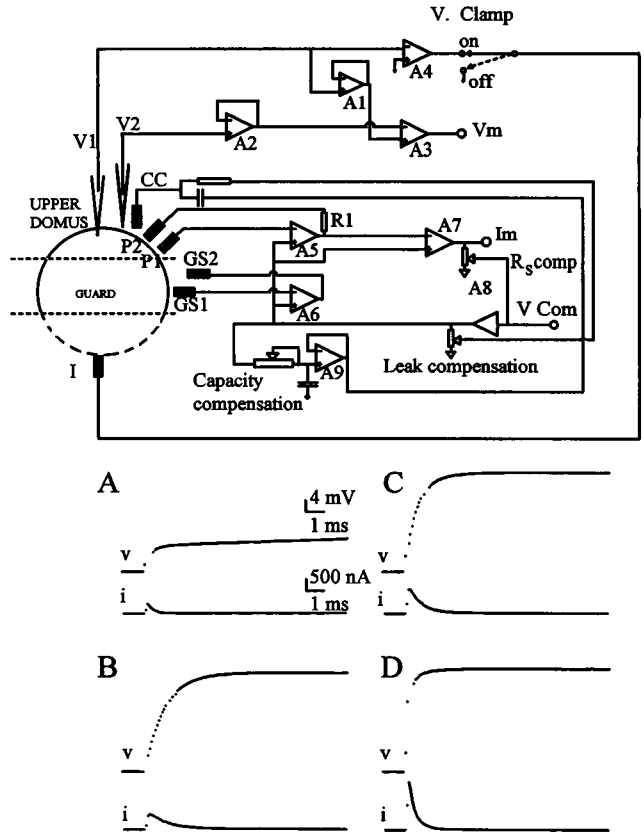

FIGURE 1 Schematic diagram of the circuitry and layout of the COVG technique (*upper panel*) and sequence of saponin permeabilization together with the reduction of cytoplasmic series resistance by the bottom insertion of a silver electrode (*bottom panel*). Control amplifiers (A1, A4, A5, and A6 were OPA 102 (Burr-Brown, Tucson, AZ)). *A* to *C* are voltage (*v*) and current (*I*) traces with *V. clamp* off. *A*, before and *B*, after saponin permeabilization. In *C* and *D*, after saponin permeabilization, a black-platinized 100 μm in diameter and sharpened silver wire was introduced from the bottom of the oocyte. In *C* ca. 700 μm in depth and in *D* just before rupture of the upper membrane. HP = −90 mV, 40-mV command pulses. The voltage was recorded between V1 and V2 placed in the vicinity. Capacity transients were fitted to a single exponential functions with time constants of 1.25 ms in *B*, 0.76 in *C*, and 0.40 in *D*. External and guard solution NaMESCa2; bottom solution KGLU + EGTA 1 mM; sampling time 50 μs per point; filter 3 kHz; one sweep per trace; R_s uncompensated; temperature 22°C. (*A*) A3810C02; (*B*) A3810C05; (*C*) A3810C14; and (*D*) A3810C15.

the command potential. The recording electrodes P1 and GS1 are placed close to the oocyte. The top pool is maintained at the command potential through a current-voltage converter amplifier A5 (via P1 and P2, *R1* = 0.1–10 MΩ), while the potential in the oocyte interior is actively clamped to ground by the feedback loop (*V1* and *V.Clamp* in the "on" configuration) between the intracellular microelectrode (inserted from the top) and the lower compartment, which is in electrical continuity with the interior of the cell by saponin permeabilization or direct rupture of the oocyte bottom membrane. The middle compartment, actively clamped to the command potential by amplifier A6 via electrodes GS1 and GS2, establishes an electrical guard between the top and the lower pool. This eliminates any voltage difference between the middle and the top compartment nulling leakage currents through the seals. Linear capacitance transients are compensated for by injecting current transients through a third bath electrode (CC) placed in the top pool (A9). The compensation has three independent time constants and amplitudes, and a phase control. The capacity compensation increases the dynamic range and prevents amplifier saturation of the control amplifiers (A4, A5, and A6). In addition, the system provides a compensation circuitry for the series resistance (R_S) in which a voltage proportional to the membrane current is added to the command pulse summing junction for A5 and A6 control amplifiers (Hodgkin et al., 1952). R_S was compensated by adjusting the speed of the capacity transient which was set prior to oscillation. Typical values for R_S are ca. 0.3 kΩ. Connections between the electronic system and the solution are made via chlorided silver wires immersed in 1–4 M NaCl pools. Agar bridges (3% agar in 0.1 M sodium methanesulfonate) with internal black platinized platinum wires, to improve the high frequency response, are used to connect the oocyte chambers with the NaCl pools.

Saponin permeabilization

The sequence of saponin permeabilization in a control oocyte is illustrated in the bottom panel of Fig. 1 which shows voltage (V) and current (I) recordings to 40 mV command pulses from HP = −90 mV. The top and guard compartments were clamped by A5 and A6, while the voltage clamp connected to V1 was off (*V.Clamp* off). In this configuration, prior to saponin permeabilization, the upper domus membrane is charged via the oocyte cytoplasmic resistance in series with the capacity and the resistance of the oocyte membrane facing the bottom chamber. In this case, the voltage responses (*A*, *v*) to the applied voltage command pulses were greatly attenuated by this combined access resistance. In *B*, after perfusing the bottom chamber with KMES + saponin (0.1%) the electrical opening of the oocyte bottom became evident from a dramatic increase of the voltage responses due to the elimination of the bottom membrane resistance; thus, under this condition, the upper domus membrane capacity was charged mainly via the oocyte cytoplasmic resistance. In this experiment, with a capacity of 39 nF and a capacity transient time constant of 1.25 ms, the calculated access resistance was 32 kΩ. The experiment also illustrates the reduction of the cytoplasmic access resistance by the bottom penetration of the oocyte with a platinized-chlorided silver wire of 100-μm diameter (before *B*, and after *C* and *D*). The silver electrode was grounded via a 1-μF capacitor. With the introduction of the silver wire ca. 700 μm in depth (*C*) and just before rupture of the upper membrane (*D*), the capacity charging time constant measured from the capacity transient was reduced from 1.25 ms in *B*, to 0.76 ms in *C* and 0.4 ms in *D*. The calculated cytoplasmic access resistance was reduced from 32, to 19.5, and 10.3 kΩ, respectively. As it will be discussed in Figs. 3 and 4, it is necessary to establish an active voltage clamp in V1 to achieve speed, since in this case, the major components of the access resistance will reside in the cytoplasm between the V1 microelectrode tip and the inner domus membrane surface.

To perfuse the interior of the oocyte, a glass capillary tube with an external diameter of 100–200 μm was introduced from the bottom. The solution was directly pumped at a flow rate of 5–50 μl/h. Internal K^+ can be totally replaced in 10–20 min by a K^+-free solution, depending on the distance between the upper domus oocyte membrane and the tip of the perfusing cannula.

Time course of the membrane capacity charge and voltage uniformity in the voltage clamped membrane area

Fig. 2 illustrates typical recordings of passive properties obtained with the COVG technique and a scheme of the microelectrode positioning. Records were obtained in the absence of R_S compensation. *A* and *B* shows the capacity (*C*) transient to a 20 mV pulse. *B* shows in an expanded time scale the sample points and the superimposed fitted curve to a single exponential with a time constant of decay of 24 μs. *C* shows the corresponding voltage recordings between the intracellular microelectrodes V1 and V3 in reference to V2 located just outside the oocyte membrane (*D*, *expanded scale*). The voltage response in V1 (voltage-clamp control microelectrode) follows the command pulse and reaches steady state in three 8-μs sample points. On the other hand, the voltage response in V3 placed close to the edge has a slower time constant (46 μs). This observation indicates that the recorded membrane currents were generated from membrane regions that reached isopotentiality between few μs and 46 μs. As a consequence, the recorded current is a weighted average of currents collected at different distances from the V1 controlling microelectrode. The capacity currents that cross the membrane near V1 have a faster time constant than the capacity currents that cross the membrane further away near the edge of the domus. This radial decay of voltage during high frequencies from the V1 electrode explains why the decay time constant of the capacity current is faster (24 μs) than

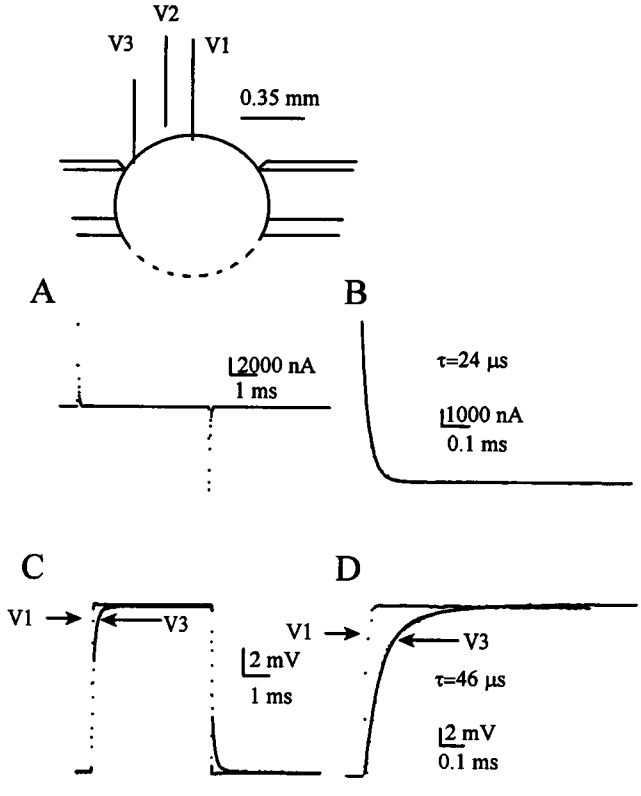

FIGURE 2 Oocyte passive electrical properties. The diagram shows the geometrical arrangement of the recording conditions. V1 microelectrode was slightly withdrawn after the penetration. *A* and *B* are capacity transients to a 20-mV pulse from −90 mV. In *B* the sample points are superimposed by a fitted exponential curve with a time constant of 24 μs. *C* and *D* (expanded scale) are the recorded transmembrane voltage responses (20-mV command pulses) of microelectrodes V1 and V3 in reference to a third external microelectrode (*V2*) placed in the vicinity. External and guard solutions NaMESCa2; bottom solution KGLU + EGTA 1 mM; saponin opened oocyte; sampling time 10 μs per point; filter 10 kHz; four sweep averages; R_s uncompensated; temperature, 22°C. (*A* and *B*) CD31C24; (*C* and *D*) CD31C14.

the time constant of the voltage jump at V3 (46 μs). Spatial uniformity can be improved by reducing the diameter of the hole in the upper recording chamber, however it makes the edge effects more important (Taglialatela et al., 1992). Typical values for a 700-μm upper whole diameter are 14- to 32-μs time constants for the capacity transient.

The value of R_S is critically dependent on the depth of penetration of the clamp control microelectrode V1 in the oocyte cytoplasm. In fact the main cause in the variability of clamp speed is given by the sharpness and the depth of the microelectrode penetration and the resulting R_S value. The traces shown in Fig. 3 were obtained after the V1 microelectrode was maximally withdrawn just before losing the recording of the membrane potential. As expected in this case, R_S had a minimum value, and its compensation did not greatly improve the capacity transient speed (not shown). Thus, to achieve maximum speed and to minimize R_S, the tip of the control V1 microelectrode has to be as close as possible to the inner oocyte membrane. Unless specified, we used a minimum level of R_S compensation (ca. 0.3 kΩ.) set just before the appearance of oscillations which did not distort ON and OFF gating current records. These measurements in the mentioned geometrical conditions set a limit of about 25 μs for the capacity transient time constant and about 50 μs to achieve spatial uniformity in the absence or large ionic currents. These values for the clamp speed should be adequate to obtain reliable measurements of *Shaker* K^+ ionic and gating currents.

Clamp homogeneity as evidenced from the time course of K^+ currents after its partial blockade by external TEA

Fig. 3 illustrates another test to evaluate clamp speed and uniformity. In these experiments we used the *Sh*H4-IR-T449Y mutation that has high external TEA sensitivity (MacKinnon and Yellen, 1990). The external solution was KMESCa2. In *A*, K^+ currents from −90 mV HP to −38 mV in subsequent 2-mV increments are shown. This voltage region near the current detection level and in the negative slope of the current-voltage relationship is very sensitive to clamp nonuniformities which can be detected as humps and discontinuities in the current records. The current traces in *A* show a gradual increase in speed and size without discontinuities indicating an adequate voltage control. Furthermore, current records in *B* from the same cell to larger potentials (−42 to −2 mV in 10-mV steps) show that tail current deactivation time constant remained invariant despite the large increase in tail current amplitude with prepulse depolarizations. Finally, records in *C* and *E* show that K^+ current partial blockade by 0.5 mM external TEA did not affect their time course. This is illustrated by superimposing scaled records with and without external TEA treatment (*D*). In other experiments performed with the *Sh*H4 clone using internal perfusion with NMG-MES with 1 mM Na_2EGTA and external NaMESCa2, we also found that inactivating K^+ currents (elicited to potentials between −20 to 40 mV from −90 mV HP) were reduced in size without changes in their kinetics as the internal K^+ was replaced. In these experiments peak currents at 40 mV ranged from 20 to 50 μA, and their time course was measured after a reduction close to 1 μA after internal perfusion (not shown). All the reported maneuvers, in addition to the fact that the time course of the ionic currents was not affected by the current amplitude, indicate that membrane currents in the ranges shown (< 20 μA) can be spatially clamped with a time resolution of at least 50 μs. This makes highly reliable the characterization of the kinetic properties of ionic currents and charge movement presented in the Results section.

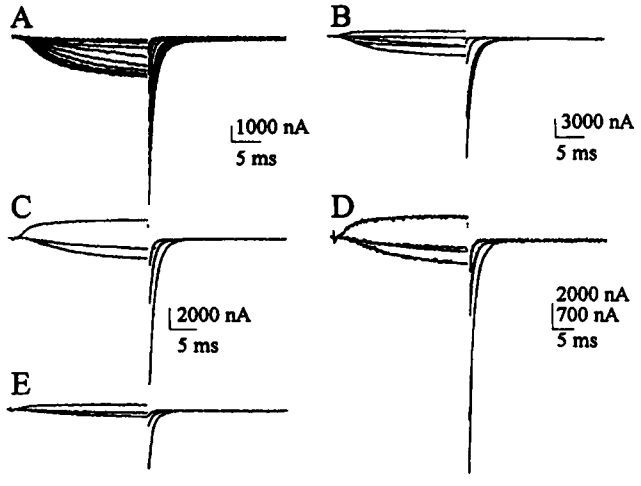

FIGURE 3 K^+ current kinetics is not affected by K^+ current amplitude. Traces are K^+ currents; HP −90 mV. (*A*) Pulses from −38 to 22 mV in 2-mV steps; (*B*) pulses from −42 to −2 mV in 10 mV steps; (*C*, *D*, and *E*) pulses to −30, −25, and 5 mV, respectively. In *E* 0.5 mM TEA was added to the external solution. (*D*) Scaled superimposed traces of *C* and *E*. The records were from *Sh*H4-IR-T449Y clone and subtracted with P/-4, SHP −90 mV. External and guard solution KMESCa2; bottom solution KGLU + EGTA 1 mM; saponin opened oocyte; sampling time 100 μs per point; filter 2 kHz; one sweep per trace; temperature, 22°C. (*A*) C3324C10; (*B*) C3324C10; (*C*) C3324C34; (*D*) C3324C34 and -C35; and (*E*) C3324C35.

RESULTS

Gating current time course in unsubtracted records

We have previously characterized *Shaker*B K^+ gating currents after eliminating K^+ ionic currents by the replacement of the cytoplasmic oocyte solution with NMG-GLU using an internal perfusion system and using subtracted records (P/-4, SHP −120 mV) (Bezanilla et al., 1991). In order to eliminate possible subtraction artifacts and to record charge movement in the presence of K^+, we maximize the expression of the mutation W434F, which we have shown eliminates ionic conduction in *Sh*H4-IR clones without major effects on gating current voltage dependence and kinetics (Perozo et al., 1993). Furthermore, we confirmed that control oocytes do not have significant charge movement. However, in some batches of oocytes (10 out of more than 100) we recorded small (5–25 nA) nonlinear transient currents that were blocked by external ouabain (100 μM), and suppressed by replacing external Na^+ with K^+ or TEA; these currents have been attributed to the Na/K pump (Rakowski, 1993). These small nonlinear currents, when present, do not significantly contaminate our gating charge records. This was confirmed by the lack of effect of Na^+-free solutions and/or ouabain on gating current records.

Large gating currents (1–10 μA at 0 mV) could be recorded 2–4 days after injection of *Sh*H4-IR-W434F cRNA. The large expression of these channels in conjunction with the high time resolution of the clamp allowed the recording of unsubtracted gating currents after a large fraction of the linear membrane capacity has been charged. Fig. 4 illustrates the main properties of *Sh*H4-IR-W434F K^+ gating currents in unsubtracted records at a fast time resolution, from HP −90 mV. The linear capacity transients are shown as the initial sample points at the beginning and end of the pulse. Gating current records show in the ON transients a monotonic decay for the pulse to −70 mV, an insinuation of a plateau phase for the pulse to −50 mV, and the appearance of a very well defined rising phase at potentials more positive than −30 mV.

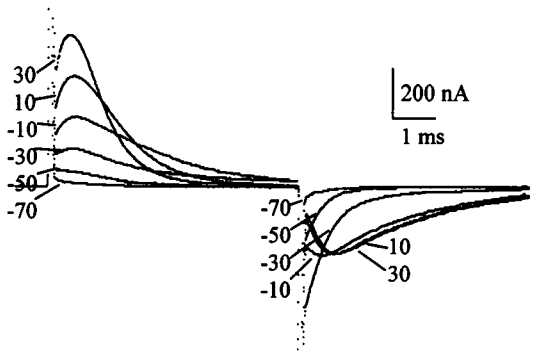

FIGURE 4 Unsubtracted gating current records. Traces are unsubtracted gating current records from *Sh*H4-IR-W434F clone; HP = −90 mV. External and guard solution NaMESCa2; bottom solution KGLU + EGTA 1 mM; saponin opened oocyte; temperature, 22°C. Sampling time 12 μs per point; filter 10 kHz; 12 sweep averages per trace. R_S was minimally compensated. Note the absence of oscillations for the −70 mV depolarizing pulse. (*C*) B2725C38.

On the other hand, the decay of the OFF transients became progressively slower with depolarizing pulses and showed a clear-cut rising phase for pulses more positive than −10 mV.

Comparison between gating charge from cut-open oocyte and cell-attached macropatches

To further establish the kinetic properties of the gating currents measured with the COVG technique, we performed equivalent measurements using the macropatch technique. Fig. 5 displays subtracted (P/-4, SHP −120 mV) (*A*) and unsubtracted (*B*) gating currents from the same oocyte using the COVG technique; as well as, subtracted gating currents obtained with the cell-attached macropatch technique (*C*). As in Fig. 4, the unsubtracted records have an initial capacity transient out of scale (few sampling points) followed by the gating currents which are practically identical with *A* and without *B* subtraction. Almost identical gating current records were also obtained with 20 mV SHP and P/4 (not shown). These results indicate that subtracted and unsubtracted gating currents measured with the COVG technique are practically indistinguishable, and confirm that negative subtracting pulses, from −120 mV SHP, generally used in gating current subtracted records are adequate (Bezanilla et al., 1991).

Records in Fig. 5 *C* were obtained in a cell-attached macropatch (6-μm internal diameter). The bath solution was isotonic K^+ (KMES + EGTA 1 mM) that sets the membrane potential close to 0 mV. The solution in the patch pipette was NMG-MESCa2. Gating current records obtained in cell-attached macropatches were very similar in their time course and voltage dependency to those obtained with the COVG. For example, for a pulse to 0 mV and at 22°C, the decay time constant was 1.5 ms with COVG and 1.8 ms with macropatch. Likewise, the *G-V* curves obtained with the COVG (Fig. 10, *G* ▼, ●) and cell-attached macropatch (Fig. 10, *G* ■) techniques under the same external solution (KMESCa2) were indistinguishable, which strengthened the validity of the measurements. Gating current records with the COVG

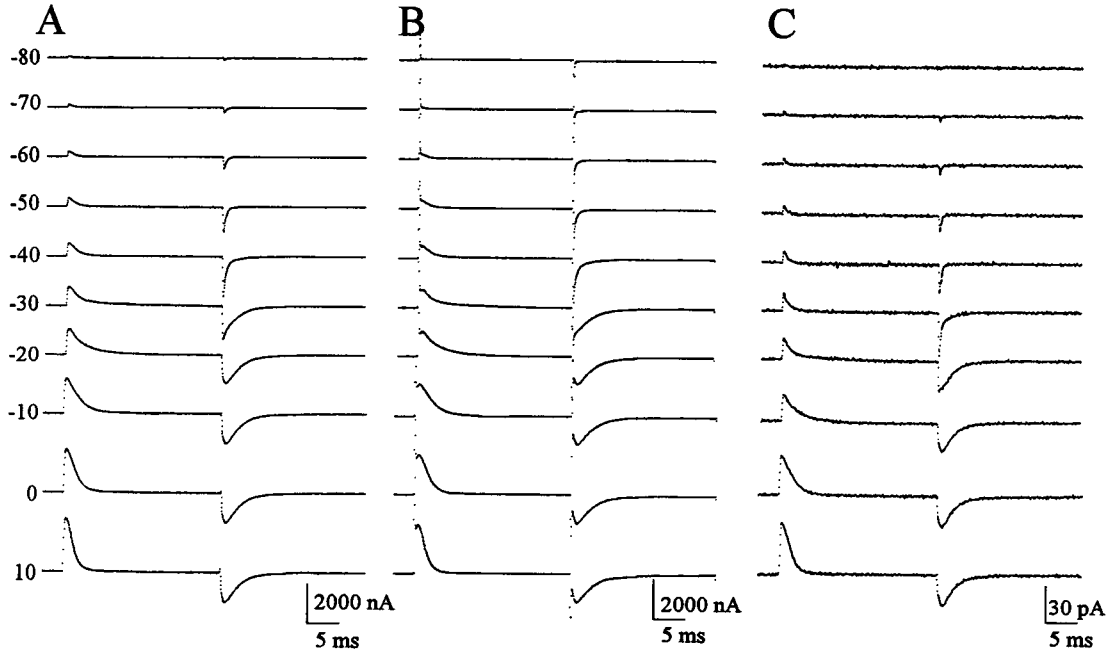

FIGURE 5 Comparison between subtracted (*A*) and unsubtracted (*B*) gating current records with the COVG technique, and subtracted records with cell-attached macropatch technique (*C*). Traces are gating current records from *Sh*H4-IR-W434F clone; HP = −90 mV. When using the COVG technique, the external and guard solution was NaMESCa2 and the bottom solution KGLU + EGTA 1 mM; saponin opened oocyte. In cell-attached macropatch the bath solution was KMES + EGTA 1 mM and the pipette solution NMG-MESCa2. Sampling time 50 μs per point; filter 5 kHz. In *A* P/-4, SHP −120 mV; in *C* P/4, SHP 20 mV. One sweep per trace in *A*, and 4 in *B*. R_S was minimally compensated in *A* and *B*. Temperature, 22°C. (*A*) B2725C01; (*B*) B2725C02; (*C*) L3405C05.

technique showed, however, some differences with those obtained with macropatches after excision; namely, the OFF gating current became progressively slower to the extent that in some cases it was difficult to separate it from the baseline noise (Stühmer et al., 1991; Schoppa et al., 1992). The slowdown of the OFF gating current induced by the macropatch excision will be treated in a future work (Sigg et al., 1994).

Voltage dependence of membrane capacity

To establish the voltage dependence of charge movement we directly measured the membrane capacity at different potentials. The additional membrane capacity introduced by the expression of ion channels was obtained from the relationship between the ON and OFF time integral under the capacity transient and the pulse potential in unsubtracted records. Fig. 6 illustrates an experiment with the nonconducting clone *Sh*H4-IR-W434F in external NaMESCa2. In *A* are unsubtracted records (HP −90 mV), *B* is the charge-voltage (*Q-V*) relationship, and *C* the capacity-voltage (*C-V*) plot obtained from *dQ/dV vs. V* from the data and fitted curve in *B*. The plot in *B* shows that the ON (●) and the OFF (▼) charge are equal, that Q is a linear function of V for potentials more negative than −110 mV and more positive than 10 mV, and that Q becomes voltage-dependent between −100 mV and 0 mV. The same applies for the voltage dependence of the capacity which shows a constant value at potentials more negative than −100 mV and more positive than 0 mV with a peak value at −37 mV (*C*). The experimental points of the *Q-V* relationship in *B* could be interpreted as the sum of a straight line (linear capacity) and a Boltzmann distribution; they were fitted to $(B + C \cdot V) + \{Q_{max}/[1 + \exp(V_{1/2} - V) \cdot (z \cdot F)/(R \cdot T)]\}$. In this expression B is the linear charge at $V = 0$ mV, C_m is the linear membrane capacity, V the membrane voltage, Q_{max} the saturating charge; $V_{½}$ the midpoint of the Boltzmann distribution, z the effective valence, and RT and F have their usual thermodynamic meanings. The best-fitted values were $B = 2.5$ nC; $Q_{max} = 5.2$ nC; $C_m = 27$ nF; $V_{1/2} = -37$ mV; and $z = 3.3$. The curve in *C* was obtained from the first derivative of Q with respect to V from the fitted curve in *B*. The experiment also illustrates that the capacity introduced by the expressed channels can be about 10 times the basal linear capacity (25 nF to ca. 200 nF). In other experiments performed in uninjected oocytes the ON and OFF

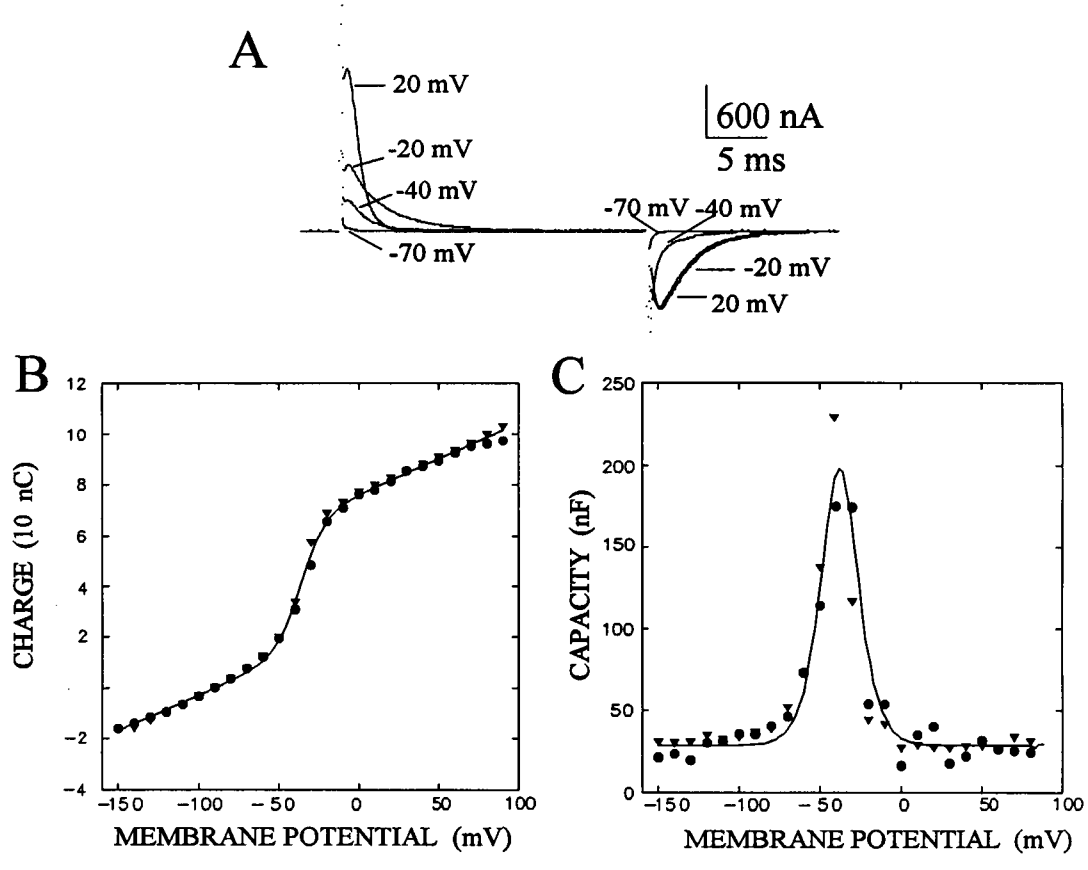

FIGURE 6 Voltage dependence of membrane capacity and charge. Traces in *A* are unsubtracted gating current records from *Sh*H4-IR-W434F clone; HP = −90 mV. (*B* and *C*) Charge-voltage and capacity-voltage relationships for ON (●) and OFF (■) transients, respectively. The charge was obtained from the time integral of the current during the pulse and the return to −90 mV HP shown in *A*. The capacity-voltage curve was obtained from $\Delta Q/\Delta V$ vs. V plots of the experimental points and fitted curve in *B*. The external and guard solution was NaMESCa2 and the bottom solution KGLU + EGTA 1 mM; saponin opened oocyte. Sampling time 50 μs per point; filter 10 kHz; four sweep averages per trace; temperature, 22°C. R_s was minimally compensated (B2725C02).

charge were linearly related to membrane voltage showing that the intrinsic oocyte membrane capacity is voltage-independent which agrees with capacity measurements in the frequency domain (Bezanilla and Stefani, 1993).

Fig. 7 shows another experiment in which we determined the capacity with small pulses (5 mV) at the end of 250-ms pulses to various potentials. In this case the linear capacity was analogically compensated at −120 mV and 0 mV. Pulses to −85, −70, and −55 mV elicited gating currents with one main component of decay; while the pulse to −40 mV shows the appearance of a second slow component of decay that follows the first fast one. These slow components become predominant for −30 and −20 mV depolarization when the channel opens (see Bezanilla et al., 1994).

The capacity at each potential was calculated from the time integral of the capacity current divided by the 5-mV pulse. The graph shows a bell-shaped dependence of the membrane capacity (●) with voltage with a peak value near −35 mV. To obtain the Q-V curve (▼), the data points of the capacity-voltage curve (●) were integrated with respect to voltage. Subsequently, the Q-V curve data points were fitted to the sum of two Boltzmann distributions of the form $Q_{1\,max}/[1 + \exp(V_1 - V) \cdot (z_1 \cdot F)/(R \cdot T)] + Q_{2\,max}/[1 + \exp(V_2 - V) \cdot (z_2 \cdot F)/(R \cdot T)]$, where $Q_{1\,max}$ and $Q_{2\,max}$ are the limiting charge movements, V_1 and V_2 the half potentials of the distribution, and z_1 and z_2 the effective valences, respectively. The best-fitted values were $Q_{1\,max} = 0.65$ nC, $V_1 = -60$ mV, $z_1 = 2.3$, $Q_{2\,max} = 1.42$ nC, $V_2 = -41$ mV, and $z_2 = 5.6$.

These observations indicate that the Q-V curves obtained from subtracted and unsubtracted traces and from the above capacity measurements were identical and could resolve two components in the charge movement. These results taken together indicate that SHP, more negative than −120 mV or more positive than +20 mV, should not introduce major nonlinearity and validate our previous measurements of charge movement with negative subtracting pulses from −120 mV and the following measurements of charge movement voltage dependence. (Bezanilla et al., 1991; Perozo et al., 1992).

Time course and voltage dependence of K^+ tail currents

We measured directly the voltage dependence of channel activation from peak tail current amplitudes at a constant potential after preceding depolarizing prepulses. This is illustrated in Fig. 8 which demonstrates the adequate time resolution for the tail current measurements and the linear current-voltage relationship for the peak tail currents. Fig. 8 (*A* and *B*) shows in KMESCa2 ionic currents elicited by pulses to 50 mV followed by postpulses to various negative potentials between −180 mV and 60 mV. In *B* the tail currents are shown in an expanded scale at 8 μs per sampling point. As in Fig. 3, tail currents are practically instantaneous at the voltage jump, and the traces do not show humps which indicate that the membrane potential during the postpulse is uniform. The graph (*D*) shows the linearity of the corresponding instantaneous current-voltage relationship. The traces in *C* illustrate the progressive increase in size of the tail currents measured at −90 mV for prepulses of increasing

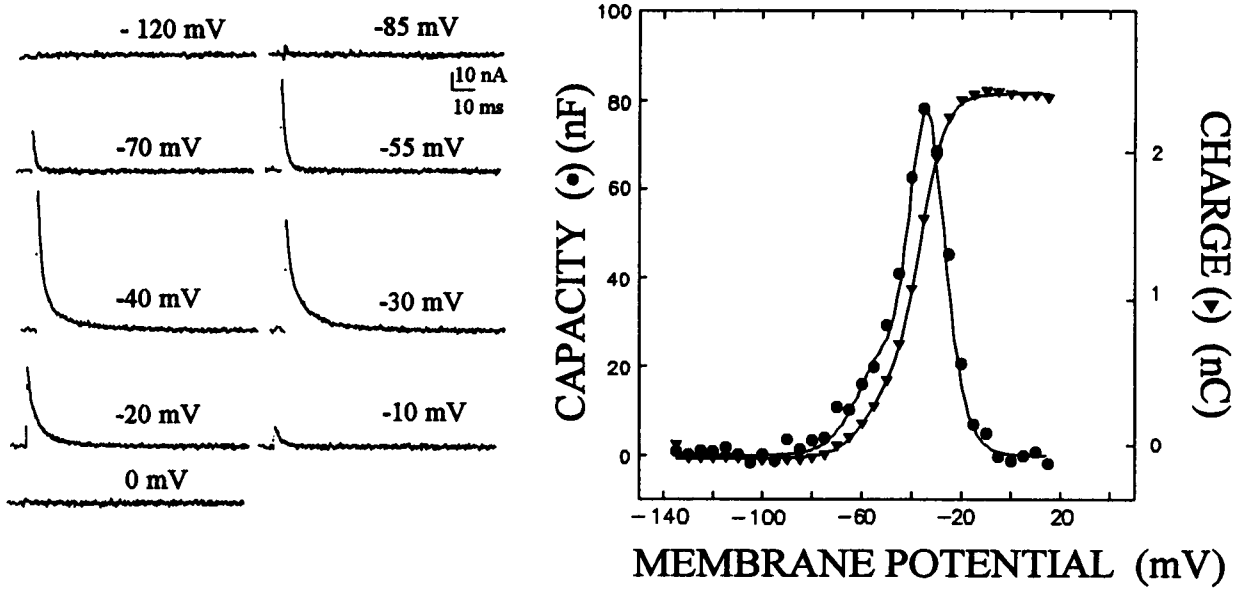

FIGURE 7 Voltage dependence of nonlinear membrane charge. Traces were analogically subtracted with 10-mV pulses at −120 mV and 0 mV HP. Examples of gating current traces to 5-mV constant pulses at the end of 250-ms prepulses to various potentials (*numbers* in *traces*) in *Sh*H4-IR-W434F clone. The experimental points in the graph were obtained from the time integral of the current during the pulse, as those shown in the traces. The capacity at each potential was calculated from this time integral of the transient current divided by the 5 mV pulse (●). The charge (▼) was numerically obtained by the voltage integral of the capacity values. These Q-V data points (▼) were fitted to the sum of two Boltzmann distributions. Finally, the capacity-voltage fitted curve was numerically calculated from the voltage derivative of the Q-V curve. The external solution was NaMESCa2 and the bottom solution KGLU + EGTA 1 mM; saponin opened oocyte; sampling time 200 μs per point; filter 1 kHz; one sweep per trace. R_S was minimally compensated; temperature, 22°C (A2017C56).

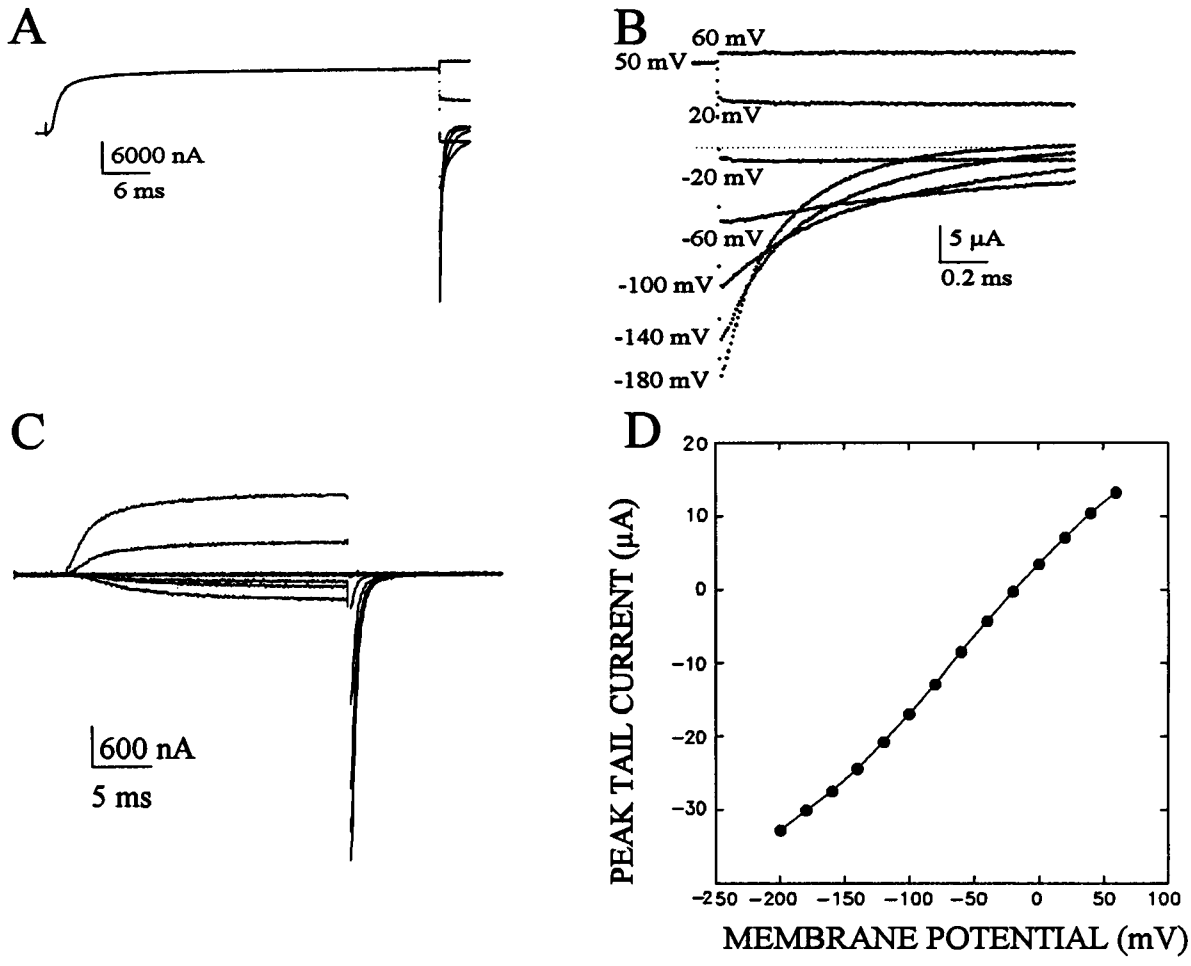

FIGURE 8 K^+ tail current voltage dependence. Traces are K^+ currents in high external K^+. (*A* and *B*) Pulses to 50 mV and postpulses from −180 to 60 mV in 40-mV increments in *Sh*H4-IR-T449Y clone, P/4, SHP −130 mV, sampling time of 100 and 8 μs per point, R_S 250 Ω; filter 10 kHz. (*C*) K^+ currents from HP = −90 mV to 10 mV in 10-mV increments in *Sh*H4-IR clone, P/4, SHP −90 mV, sampling time of 50 μs per point, R_S minimally compensated; filter 5 kHz. *C* is the instantaneous current-voltage relationship measured at the peak of tail currents from *A* and *B*. *A* shows the whole trace, while *B* shows the OFF tail responses in an expanded time scale. The peak tail current is established in two sample points. External and guard solution KMESCa2; bottom solution KGLU + EGTA 1 mM; saponin opened oocyte; one sweep per trace; temperature, 22°C. (*A* and *B*) C3324C31; (*C*) B3513c16.

amplitudes. The records also show the practically invariant decay time at a constant return potential (−90 mV) and for tail currents of different amplitudes (*C*) and the faster decay time with more negative return potentials (*A* and *B*).

The tail current time course, which reflects the K^+ channel closing upon repolarization, gives indication on the transitions from the open state(s) to the closed state and it is a sensitive parameter for channel model function when compared with the associated OFF charge movement relaxation. Fig. 9 shows deactivation K^+ tail currents in external Na^+ (*left*) and K^+ (*right*) solutions in a *Sh*H4-IR clone. At the termination of the 20-mV pulse, when the membrane potential was stepped back to −80 mV, outward (*A*) and inward (*B*) K^+ tail currents were recorded in external Na^+ or K^+, respectively. The bottom panels (*C* and *D*) show the corresponding K^+ tail currents in an expanded scale with the superimposed fitted curves. For comparison, the record in *D* was inverted. Deactivation tail currents in both ionic conditions could be described by the sum of two exponential functions. The first component had a time constant faster than 0.5 ms, while the second component had a time constant of about 2 ms. These dual deactivation time constants do not necessarily indicate the presence of two classes of channels or two different open states, since two time constants in the deactivating tails can be predicted from a simple sequential model with concatenated closed states and one final open state (see Bezanilla et al., 1994). Another finding was that high external K^+ slows down the channel closing, in this case by slowing the decay of the first predominant component. A similar finding was reported for the squid giant axon delayed rectifier and was interpreted as channel closing being partially prevented by the presence of K^+ at some locus of the channel (Swenson and Armstrong, 1981).

Voltage dependence of charge movement and K^+ channel opening

Fig. 10 shows the steady state charge-voltage (*Q-V*) and conductance-voltage (*G-V*) relationships. We have found that the kinetics of gating currents and macroscopic ionic

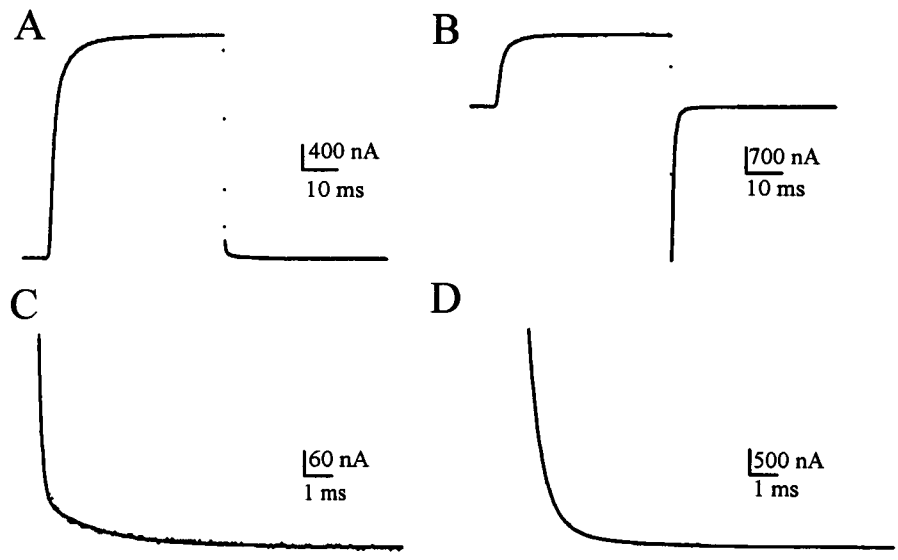

FIGURE 9 Deactivation K^+ tail currents in external Na^+ (*left*) and K^+ (*right*) solutions. Traces are from *Sh*H4-IR in external NaMESCa2 (*A* and *C*) and KMESCa2 (*B* and *D*). Pulses are to 20 mV from HP = −90 and stepped back to −80 mV. Traces in *C* and *D* are expanded records and superimposed fitted traces of deactivation tails. *D* is inverted. Deactivation K^+ currents were fitted to the sum of two exponentials. In *C*, $a1 = 0.77$, $\tau 1 = 0.13$ ms, $a2 = 0.23$ and $\tau 2 = 2.04$ ms; in *D* $a1 = 0.87$, $\tau 1 = 0.49$ ms, $a2 = 0.13$ and $\tau 2 = 1.90$ ms, where $a1$ and $a2$ are amplitude factors and $\tau 1$ and $\tau 2$ the time constants. External and guard solution NaMESCa2 in *A* and *C*; and KMESCa2 in *B* and *D*; bottom solution KGLU + EGTA 1 mM; saponin opened oocyte; temperature, 22°C. Sampling time 100 μs per point; filter 2 kHz; one sweep averages per trace. R_S was minimally compensated (B3513C08 and -C09).

currents vary between oocytes. This makes impossible a quantitative comparison of gating currents kinetics and ionic currents kinetics unless it is done in the same patch of membrane. We have found however, that the steady state properties are much less variable from oocyte to oocyte, and this allowed us the comparison shown in Fig. 9. In fact, in this figure, the gating charge (Q) corresponds to the plotted charge in the nonconducting W434F clone (●) and in the normal conducting H4-IR (▼, ■) where the determination could be made for potentials negative enough that did not show ionic currents. The experimental points obtained every 2 mV closely follow the same Q-V curve and are indistinguishable between the conducting and nonconducting clones. Charge movement at potentials more negative than −40 mv increased slowly with voltage, while at more positive potentials than −40 mV, when channel opening occurs, it becomes more steeply voltage-dependent, and finally tend to saturate at potentials more positive than −20 mV.

The Q-V relationship has a different steepness at negative potentials, where it starts, and at positive potentials, where it tends to saturate. As a consequence, the data points of the Q-V relationship could not be well described by a single Boltzmann distribution as shown by the curve in the graph that separates from the data points at more negative potentials ($V_{1/2} = -35$ mV, $z = 3.0$). The experimental points can be better described by the sum of two Boltzmann distributions with $Q_{1\max} = 0.44$, $V_1 = -47.4$ mV, $z_1 = 1.96$, $Q_{2\max} = 0.56$, $V_2 = -34.3$ mV, and $z_2 = 5.16$.

To correlate charge movement with channel opening we obtained the steady activation curve by directly plotting in high external K^+ the peak tail current amplitude at a constant postpulse potential ($V_1 = -90$ mV), and as a function of a test prepulse potential, V (see Fig. 8 *C*). In this case, at the termination of the prepulse the current jumps to a new value due to the abrupt change in the K^+ driving force. During this brief time interval after the end of the prepulse the number of open channels at the peak tail amplitude remains the same; thereafter the K^+ tail current decays as the channels close. The ionic current amplitude is given by

$$I(V, V_1) = Ni(V_1)P_o(V)$$

where $I(V, V_1)$ is the total ionic membrane current at the peak of the tail, $i(V_1)$ is the single channel current at the constant pulse potential V_1, $P_o(V)$ is the probability of channel opening at the end of the pulse of amplitude V and N is the number of channels in the oocyte membrane domus. Since N and $i(V_1)$ have constant values, normalized $P_O(V)$ values could be obtained by dividing peak tail current amplitudes obtained with different prepulses by the limiting peak tail current value with the largest prepulse (V_m)

$$I(V, V_1)/I(V_m, V_1) = P_o(V, V_1)/P_o(V_m, V_1) = P_O(V) \quad (1)$$

With this method, the computed normalized $P_O(V)$ value is equivalent to the normalized macroscopic conductance $G(V)$. The experimental data at the right in Fig. 9 (*G*) shows normalized tail current peak amplitudes in *Sh*H4-IR K^+ channel in high external K^+ with the COVG (●, ▼) and macropatch (■) techniques.

The important features of the Q-V and G-V curves are: (i) a sizable amount of charge moves in the negative region where no conductance is observed, (ii) the potential at which the Q-V curve becomes steeper corresponds to the potential at which the conductance is first observed and the apparent steepness of the conductance is similar to the steepness of this region of the Q-V curve, and (iii) the charge seems to saturate

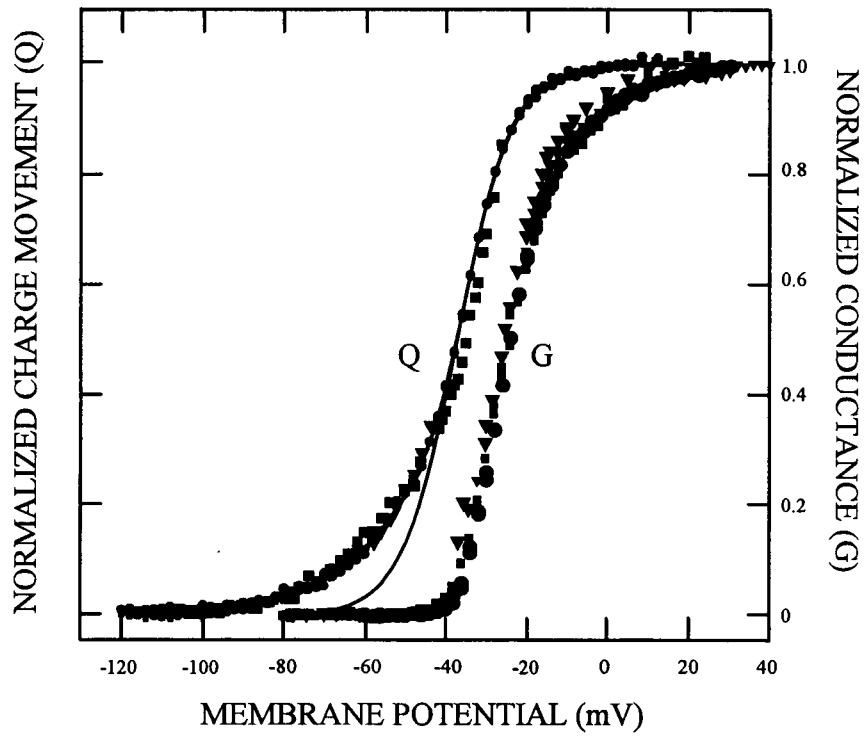

FIGURE 10 *Q-V* and *G-V* curves in ShH4-IR and ShH4-IR-W434F clones. The K^+ conductance (*G*) was obtained from tail current amplitudes measured after after stepping back to −90 mV from 36-ms (▼), 40-ms (■), and 50-ms (●) depolarizing pulses (*Sh*H4-IR, P/-4, SHP −90 mV). External solutions were Na55-TEA55 MESCa2 (●) and KMESCa2 (▼, ■); the COVG (●, ▼) and macropatch (■) techniques were used. In cell-attached macropatch the bath solution was KMES + EGTA 1 mM. The ON charge movement (*Q*) was measured in the nonconducting clone *Sh*H4-IR-W434F in external NaMESCa2 and internal KGLU from −120 to +16 mV (●); and in the conducting clone *Sh*H4-IR from −120 mV to −50 mV (▼) in the same solution and in external TEAMESCa2 and internal TEAGLU from −120 mV to −20 mV (■). Charge movement data points were normalized to match the relative charge at −50 mV. P/-4 with SHP −120 mV and saponin opened. Temperature, 22°C (files A2D17C05 to -09; F3403C03; C3324C03, A3116C08 to -14; and C3126C24 to -26).

at more negative potentials than the conductance which shows a prominent creep between 0 and +30 mV while the charge is essentially flat.

Ionic and gating currents are equally time-shifted by changing the initial conditions

Cole and Moore (1960) reported that K^+ currents were delayed by hyperpolarizing prepulses. A similar phenomenon found for Na^+ currents was, in addition, correlated with an equivalent shift of the Na^+ gating currents. This correspondence in the time shifts of ionic and gating currents gave a strong argument in favor of the hypothesis that most of the charge movement, including the one occurring at very negative potentials and prior channel opening, is associated with the opening of the Na^+ channel (Taylor and Bezanilla, 1983). In this section, after having established the validity of the ionic and gating current measurements, we describe similar maneuvers to compare the effect of initial conditions on the time shifts of ionic currents and charge movement. Fig. 11 shows the effect of different duration and amplitude prepulses on the delay and time course of ionic and gating current records from *Sh*H4-IR (*A*, *upper traces*) and *Sh*H4-IR-W434F (*A*, *lower traces*) clones, respectively. In *A*, pulses to 20 mV from HP = −90 mV were preceded by depolarizing (A1 and A3) and hyperpolarizing (A2 and A4) pulses. The traces show unambiguously that the depolarizing prepulses produced a left time shift of the ionic current onset. On the other hand, the same prepulses did not affect the gating current onset, but made the onset of the decay phase earlier without major changes in the time course. Hyperpolarizing pulses had the opposite effects on both ionic and gating currents (A2 and A4). In addition, as previously shown in Fig. 4, we confirmed that *Shaker* K^+ gating currents had a well defined rising phase from HP = −90 mV (Fig. 11, *right trace* in A3), and that depolarizing prepulses reduced the rising phase while hyperpolarizing ones made it more prominent (Perozo et al., 1992; Bezanilla et al., 1994).

To evaluate the time shifts we measured the time of the half maximum amplitude for the ascending phase for the ionic currents and descending phase for gating currents, and referred those times to their values without prepulses (HP = −90 mV). Negative numbers mean a left shift while positive ones the opposite. To illustrate the time course of the shift development at various prepulse potentials, Fig. 11 depicts K^+ ionic (*B*) and gating (*C*) current delays versus prepulse durations at various prepulse potentials. One striking feature of these plots is the similar time course for both ionic and gating current time shifts at similar potentials. In both cases the process had a slower time course at more depolarized potentials, and tended to saturate and become faster at negative potentials close to −120 mV. This last observation agrees with the lack of noticeable charge movement at potentials more negative than −120 mV. To compare the ionic and gating current time shifts, we plotted in *C* ionic versus gating current time shifts for equivalent prepulses. The linear relationship thus obtained demonstrates a clear correlation between gating and ionic currents.

DISCUSSION

We have studied the kinetics and steady state properties of ionic and gating currents in *Shaker* K^+ channels expressed in *Xenopus* oocytes using the COVG technique. The advantages and limitations of this technique will be discussed first, followed by a discussion on ionic and gating currents char-

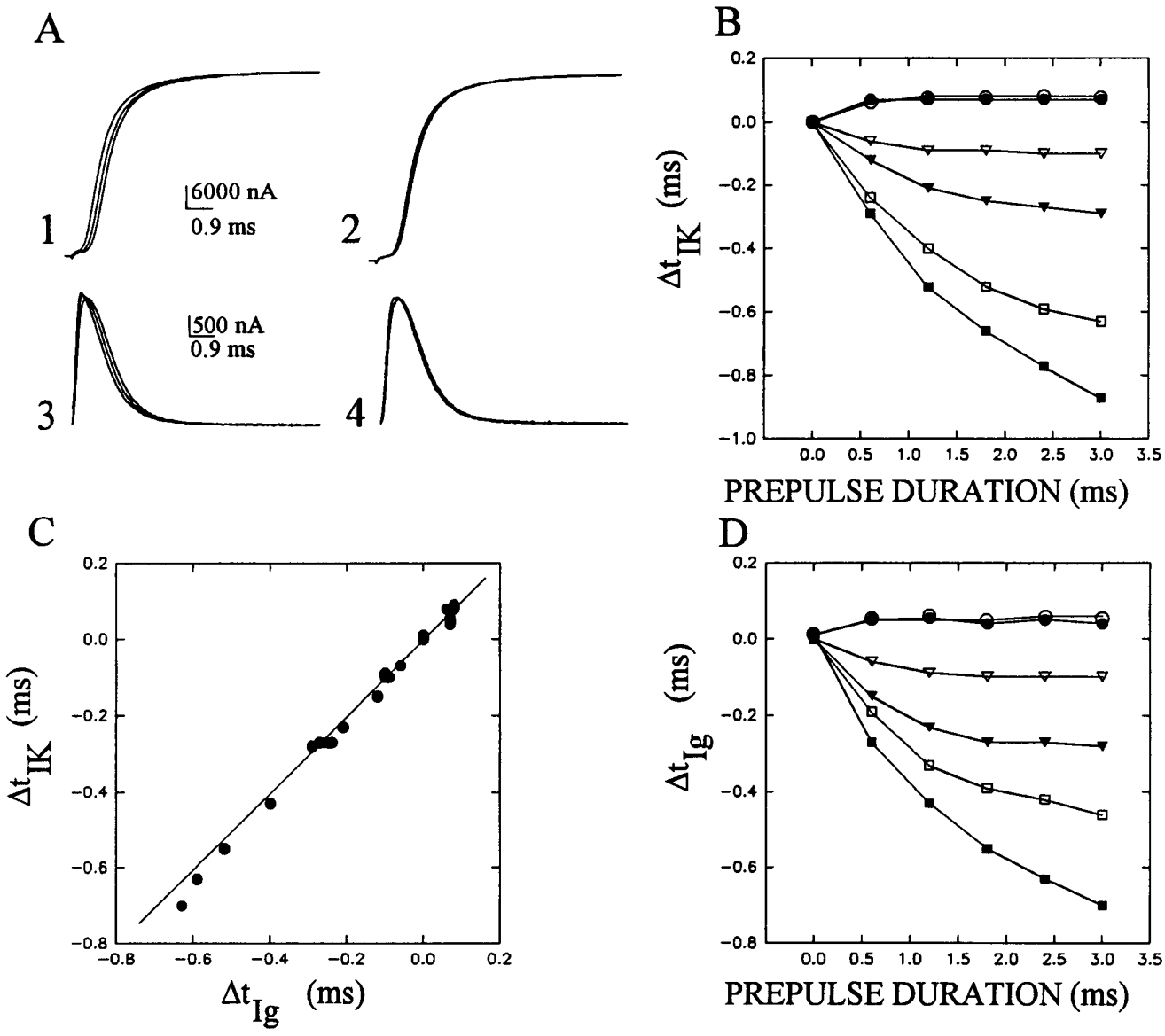

FIGURE 11 Effect of prepulse durations and amplitudes on the time course and latency of K^+ ionic and gating currents. (*A*) Traces are ionic (*upper*) gating (*lower*) current records from *Sh*H4-IR and *Sh*H4-IR-W434F clones, respectively. Pulses to +20 mV from HP = −90 mV were preceded by 0.6- and 3-ms prepulses to −50 mV (*A1*), −130 mV (*A2*), −50 mV (*A3*), and −120 mV (*A4*). In A1 and A3 the traces at the right and in A2 and A4 traces at the left did not have prepulses. (*B* and *D*) Plots of the K^+ ionic and gating current delays versus prepulse durations at various potentials. The measurements were referred to the delay at −90 mV. The delay was measured as the time at half maximum amplitude for the ascending phase for the ionic currents and descending phase for gating currents. In *B* prepulse potentials were −130 mV (○), −110 mV (●) 70 mV (▽), −50 mV (▼), −30 mV (□) and −10 mV (■); while in *D* −120 mV (○), −110 mV (●), −70 mV (▽), −50 mV (▼), −40 mV (□), and −30 mV (■). (*C*) Shows the linear correlation between ionic and gating current delays for prepulses with same amplitudes and durations. External and guard solution was NaMESCa2 and the bottom solution KGLU + EGTA 1 mM; saponin opened oocyte. Sampling time 12 μs per point; filter 10 kHz. P/-4, SHP −140 mV. Sweeps are single traces. R_S was minimally compensated. Temperature 22°C. A1 and A2, A2725C09 to -C12; A3 and A4, B2725C17 and -C18.

acteristics that are important in understanding the activation of the K^+ channel conductance.

The cut-open vaseline gap technique and the linearity of the oocyte membrane

The main difficulty in obtaining reliable voltage clamp current measurements is the presence of high R_S and resulting spatial nonuniformities (Taylor et al., 1960; Bezanilla et al., 1982). The COVG technique in which the membrane domus is clamped with a current source close to the center of the sphere should benefit from the spherical symmetry to achieve a fast and homogeneous clamp. The evaluation of the speed and homogeneity with a second intracellular electrode (V3) near the edge of the domus (ca. 300 μm from the voltage control microelectrode V1) showed that in the absence of R_S compensation 1) the voltage response recorded in V1 followed the time constant of the command pulse (1–5 μs), 2) the voltage response recorded close to the domus edge (V3) had a finite time constant of 40–50 μs, and 3)

the time constant of decay of the capacity current was somewhat faster (20–30 μs) than the voltage response at V3.

Ideally, a point current source located at the center of the oocyte with spherical geometry should generate concentric isopotential layers with decaying potential values from the injecting point. With this geometry, the tip of the voltage control electrode (V1) should record one of those isopotential layers close to the surface membrane; the difference between the potential recorded by the tip of the electrode and the potential next to the membrane is proportional to the R_S value which should be possible to compensate. Under these conditions, the decay time constant of the capacity current would be $\tau = C_m \cdot (R_m \cdot R_S)/(R_m + R_S)$ which is close to R_sC_m. In this case the main component of the R_S should arise from the distance between the V1 recording point and the inner surface membrane of the domus, and the R_S value can be calculated from $R_S = \tau/C_m$ being ca. 1 kΩ (1.03 kΩ in Fig. 2). Since the time constant of the capacity transient was always slower than the time constant of the command pulse, it indicates lack of spherical geometry and it is consistent with the slower voltage response recorded by the V3 microelectrode near the edge of the domus; i.e., the lack of isopotentiality in the layer next to the inner membrane domus due to a distributed R_s. From K^+ tail measurements R_S could be maximally compensated with values ranging from 250 to 500 Ω. These results show that the cable properties of the oocyte membrane domus set an important limit for the clamp speed which is in the range of 10 kHz, an adequate bandwidth for the recordings of *Shaker* K^+ ionic and gating currents.

Measurements of nonlinear charge movement

To evaluate the measurements of gating currents, we initially tested the linearity of the oocyte membrane. Oocyte membranes in control oocytes had in most cases undetectable nonlinear capacity and resistive components. These experiments were performed in the voltage range between −110 to 30 mV, in the absence of external Cl^-, and with 2 mM external Ca^{2+} (NaMESCa2). In this solution, endogenous inward Ca^{2+} currents remain unresolved, however, in some cases their presence could be detected indirectly as a slow inward Cl^- tail when returning to −90 mV after depolarizing pulses to 0 mV (Miledi, 1982; Barish, 1983). Larger depolarizations approaching the Ca^{2+} equilibrium potential reduced these inward tail currents. The size of these inward Ca^{2+} dependent tails ranged from 0 to 5 nA and should not introduce a significant error in our gating current recordings which ranged from 500 nA to 10 μA at 0 mV. Another nonlinearity in these recording conditions was the presence of ON and OFF Na/K pump transient currents blocked by ouabain and the removal of external Na^+ (Rakowski, 1993). These nonlinear transient currents were very infrequent, depending on the batch of oocytes, and also exceedingly small (5–20 nA at 0 mV), and should not appreciably alter our *Shaker* K^+ channel gating current recordings. These assumptions were confirmed by the fact that *Shaker* K^+ gating currents were not affected by conditions that removed endogenous Ca^{2+}, Ca^{2+}-dependent Cl^-, and Na/K pump currents. These conditions were external ouabain (100 μM) and the replacement of external sodium by K^+ for the Na/K pump.

The usual procedure to separate nonlinear charge movement from linear capacity and resistive membrane components is by subtraction of small current scaled current pulses in potential ranges in which the membrane capacity and resistance is largely voltage-independent (Bezanilla and Armstrong, 1977). This has been successfully applied to record gating currents for Na^+ and K^+ channels in the squid giant axon and in other tissues (i.e., Bezanilla and Armstrong, 1977; White and Bezanilla, 1985; Spires and Begenisich, 1989; Taglialatela and Stefani, 1993). To characterize *Shaker* K^+ channel gating charge movement we have used a P/-4 protocol from −120 mV SHP, after verifying that the membrane components were voltage-independent in that region (Bezanilla et al., 1991). The fact that subtracted (P/-4, SHP −120 mV and P/4, SHP 20 mV) and unsubtracted records had equal features in terms of their voltage dependence and time course confirm the adequacy of the subtracting protocol that we have used, and established beyond any doubt, the presence of a rising phase in the ON and OFF gating currents (Bezanilla et al., 1991; Perozo et al., 1992; Taglialatela and Stefani, 1993). Furthermore, the charge movement voltage dependence was confirmed from capacity measurements with small and large pulses. These experiments indicated that the capacity became invariant at potentials more negative than −100 mV which validated the subtraction protocols used.

Nonlinear charge movement in macropatches

An important result was the similarity of the gating currents recorded with the COVG and cell-attached macropatch techniques. However, the cause of the slow OFF gating current records obtained with excised macropatches remain unexplained. Recently Stühmer et al. (1991) and Schoppa et al. (1992), recorded charge movement with excised macropatches with a very small, or practically absent, OFF charge. The results of Stühmer et al. (1991) have been explained by the presence of internal TEA and slow deactivation of the channel clone they used (Bezanilla et al., 1991; Perozo et al., 1992; Perozo et al., 1993). However, this cannot be the case in the experiments performed by Schoppa et al. (1992) in which the OFF charge movement was practically absent, and the records were performed in the absence of internal TEA and in a regular *Shaker* K^+ channel clone with the inactivation removed. Since charge movement records in macropatches performed in the cell-attached mode had identical properties to the charge movement records obtained with the COVG technique, we speculate that patch excision may result in

some alteration in the internal milieu of the cytoplasmic phase which produces a progressive slowdown of the charge movement. This presumption agrees with recent observations in which we have noted a progressive slowdown of the OFF charge movement, and of the inward K^+ tail currents after patch excision (Sigg, Bezanilla and Stefani, in preparation).

Voltage dependence of charge movement and membrane capacity

We have taken advantage of the nonconducting W434F mutant of the *Sh*H4-IR to study the details of the *Shaker* K^+ channel charge movement. The most obvious expression of the nonlinear properties of this charge movement is shown in Fig. 6 *B*, where the integral of the current is plotted as a function of the membrane potential. The charge transported negative to −100 mV is a linear function of the voltage as well as the charge moving at potentials more positive than 0 mV. The nonlinear region in between coincides roughly with the nonlinear activation of the ionic currents in the conducting mutant. This nonlinear charge has all the characteristics of a capacitive charge: its time course is transient and all the charge moved during the pulse is moved back at the end of the pulse (Fig. 6 *B*). The capacitance responsible for this nonlinear charge was estimated as the first derivative of the *Q-V* curve of Fig. 6 *B* and plotted in Fig. 6 *C*. A direct measurement of the capacitance $C(V)$ was done by applying small perturbing pulses of amplitude v at different potentials (V) (Fig. 7). The value of $C(V)$ was computed from the ratio $q(V)/v$, where $q(V)$ is the area of the current transient for the perturbation v at the voltage V. The $C(V)$ is plotted in Fig. 7, right panel and it is an asymmetrical bell-shaped curve, indicating that a simple Debye relaxation is not enough to account for the data. Two components in the voltage dependence of the capacitance are required as a minimum, consistent with the results obtained in the frequency domain (Bezanilla and Stefani, 1993). The two components are also expressed as two relaxations in the current transients recorded for small perturbations (*left panel* of Fig. 7). It is important to note that the results obtained with small perturbation analysis agree with the results obtained with large pulses, indicating that, during the time required to do the measurement, the voltage dependence of the charged particles or dipoles is stationary. This property is used to propose the basic markovian model presented in the next paper (Bezanilla et al., 1994). A verification of the equivalence of both methods is shown by the integral of $C(V)$ *vs.* V which gives a *Q-V* curve not fitted by a simple Boltzmann distribution (*right panel* of Fig. 7). The maximum value of $C(V)$ may be as large as 10 times the membrane capacity of the oocyte as it is shown in Fig. 6, giving an excellent separation of the intrinsic capacitance and the channel-induced capacitance, which allows the recording of gating currents without subtraction (see Fig. 4).

The relation between gating currents and channel opening

In establishing the link between the gating charge movement and the channel opening, it is important to estimate the open probability reliably. Most of the tests done on the clamp system explained above were aimed to assure a reliable measurement of the kinetics of the ionic currents even when currents were as large as 20 μA. The current tails shown in Fig. 8 indicate that we can measure the instantaneous I–V of the channel and also determine the voltage dependence of the conductance. As shown under Results, the method used to measure the conductance estimates directly the relative open probability of the channel, which is the voltage-dependent property of the channel that must be correlated with the voltage dependence of the charge movement. The correlation of the charge with the conductance was done mainly with the steady-state properties, because they show less variability than the kinetics. However, some qualitative aspects of the ionic currents were described in detail because they set important limits and restrictions to the modelling of channel gating. In particular, we studied the kinetics of the current turn-on as a function of the initial conditions (see below) and the kinetics of the currents during repolarization. Fig. 9 shows examples of ionic current tails in normal and high external potassium. The striking feature is the double exponential decay of the current tail. The *Shaker* K^+ channel is known to have only one open state, therefore the double exponential must be the result of a finite forward rate between the last closed and the open state that originates two eigenvalues in the current tail decay (see Goldman, 1991). This result will be an important prediction of the model developed in the next paper based only on gating current. The relative values of the voltage dependence of the rate constants between the last two closed and the last closed states are critical in reproducing the double exponential in the ionic current tails (Bezanilla et al., 1994). The two exponential components are also observed in the high external potassium, where the fast component is slowed down but the slow component remain unchanged (see legend of Fig. 9). We may ascribe the first (fast) component to the eigenvalue mainly generated by the rate going from the open to the last closed state and the second (slower) component to the eigenvalue close to the rate between the two consecutive closed states. In that case, the slowing down of the first component by high external potassium could be correlated with the presence of K^+ ions in the channel mouth as was indicated by Swenson and Armstrong (1981).

From the *Q-V* curves it is clear that a simple Boltzmann does not fit the data. Although the components of the charge versus potential distribution will be studied in detail in the next paper we need to emphasize here the aspects of the relation that help in the correlation between the charge movement and channel opening. Thus, at potentials more negative than −40 mV, about a third of the charge has moved but the conductance is practically zero (Fig. 10). The obvious question is whether the charge moving negative of −40 mV has any relation to the opening of the

channel. The experiments with prepulses using the basic protocol of Cole and Moore (1960) were designed to explore the involvement of the charge movement between −100 and −40 mV in channel gating. In Fig. 11 *B* the establishment of the shift of the potassium current with prepulse duration for different amplitudes is the same as the shift in gating current shown in Fig. 11 *D* and the summary of the correlation is shown in Fig. 11 *C* where shifts are seen to be equivalent for ionic and gating currents. Although the shifts are the same, the effects of prepulses are different in the kinetics of the ionic versus gating currents. The ionic currents show a more pronounced lag in the turn on as the prepulse is more hyperpolarized and, in contrast, the gating currents develop a more pronounced rising phase. When the prepulse is depolarizing, the delay decreases for the ionic current and the rising phase tends to disappear in the gating current. This result is important because it helps to determine the characteristics of the charge movement in the region of potential where the Cole-Moore shift takes place. In particular, the development of the rising phase is indicative of initial steps carrying less charge than later ones, a property that will be crucial in the modelling of the gating process presented in the next paper. As the movement of this charge is correlated with a prolonged delay in the ionic current, we may assign this charge movement to transitions between closed states that must precede channel opening. It is then concluded that the Cole-Moore type of experiments shown in Fig. 11 show that the charge moving in the negative region is indeed directly involved in channel activation, but not the channel opening, and it must be made of steps carrying smaller amount of charge than the steps occurring more positive than −40 mV.

The charge moving at potentials more positive than −40 mV seems to correlate well with the voltage dependence of the normalized open probability. However, at potentials more positive than −10 mV, the charge seems to saturate, while the $P_O(V)$ is still increasing with voltage (Fig. 10). This result speaks in favor of a step leading into the open state carrying less charge than the previous steps. As this last transition would contribute with less charge than all the previous ones, it would become undetectable in the Q-V curve and at the same time the P_O would not be maximum, because the channels would only open when this last step occurs. In agreement with this interpretation is the double exponential decay of the deactivation tails that require a finite forward rate in the last step, a consequence of the shallow voltage dependence of that transition. The features of the charge and the P_O are complex enough that a detailed correlation may only be possible after a quantitative description of the gating current becomes available and this is the main purpose of the next paper (Bezanilla et al., 1994).

Supported by United States Public Health Services Grants GM30376 (to F.B.), HL37044 (to E.S.), and HL47382 (to L.T.). E.P. was supported by the Pew Charitable Trust.

REFERENCES

Armstrong, C. M., and F. Bezanilla. 1973. Currents related to movement of the gating particles of the sodium channels. *Nature (Lond.)*. 242:459–461.

Barish, M. E. 1983. A transient calcium-dependent chloride current in the immature *Xenopus* oocyte. *J. Physiol.* 342:309–325.

Bezanilla, F. 1985. Gating of sodium and potassium channels. *J. Membr. Biol.* 88:97–111.

Bezanilla, F., and C. M. Armstrong. 1977. Inactivation of the sodium channel. I. Sodium current experiments. *J. Gen. Physiol.* 70:549–566.

Bezanilla, F., E. Perozo, D. M. Papazian, and E. Stefani. 1991. Molecular basis of gating charge immobilization in Shaker potassium channels. *Science (Wash. DC)*. 254:679–683.

Bezanilla, F., E. Perozo, and E. Stefani, 1994. Gating of Shaker K^+ channels: II. The components of gating currents, and a model of channel activation. *Biophys. J.* 66:1011–1021.

Bezanilla, F., and E. Stefani. 1993. Capacitance induced by Shaker K^+ channel. *Biophys. J.* 64:A114. (Abstr.)

Bezanilla, F., J. Vergara, and R. E. Taylor. 1982. Voltage clamping of excitable membranes. In *Methods in Experimental Physics*, Vol. 20. G. Ehrenstein and H. Lecar, editors. Academic Press, Inc., New York. 445–511.

Cole, K. S., and J. W. Moore. 1960. Potassium ion current in the squid giant axon: dynamic characteristics. *Biophys. J.* 1:161–202.

Fu, L., R. Ye, L. W. Browder, and R. N. Johnston. 1991. Translational potentiation of messenger RNA with secondary structure in *Xenopus*. *Science (Wash. DC)*. 251:807–810.

Goldman, L. 1991. Gating current kinetics in *Myxicola* giant axons. Order of the back transition rate constants. *Biophys. J.* 59:574–589.

Hodgkin, A. L., A. F. Huxley, and B. Katz. 1952. Measurement of current-voltage relations in the membrane of the giant axon of Loligo. *J. Physiol.* 116:424–448.

Hoshi, T., W. N. Zagotta, and R. W. Aldrich. 1991. Biophysical and molecular mechanisms of Shaker potassium channel inactivation. *Science (Wash. DC)*. 250:533–538.

Kamb, A., J. Tweng-Drank, and M. A. Tanouye. 1988. Multiple products of the *Drosophila* Shaker gene may contribute to potassium channel diversity. *Neuron.* 1:421–430.

MacKinnon, R., and G. Yellen. 1990. Mutations affecting TEA blockade and ion permeation in voltage-activated K^+ channels. *Science (Wash. DC)*. 250:276–279.

Methfessel, C., V. Witzemann, T. Tahashi, M. Mishina, S. Numa, and B. Sakmann. 1986. Patch clamp measurements on *Xenopus laevis* oocytes: currents through endogenous channels and implanted acetylcholine receptor and sodium channels. *Pflüger Arch.* 407:577–588.

Miledi, R. 1982. A calcium-dependent outward current in *Xenopus laevis* oocytes. *Proc. R. Soc. Lond. B.* 215:492–497.

Perozo, E., D. M. Papazian, E. Stefani, and F. Bezanilla. 1992. Gating currents in Shaker K^+ channels. Implications for activation and inactivation models. *Biophys. J.* 62:160–171.

Perozo, E., R. MacKinnon, F. Bezanilla, and E. Stefani. 1993. Gating currents from a non-conducting mutant reveal open-closed conformations in Shaker K_+ channels. *Neuron.* 11:353–358.

Rakowski, R. F. 1993. Charge movement by the Na/K pump in *Xenopus* oocytes. *J. Gen. Physiol.* 101:117–144.

Schneider, M. F., and W. K. Chandler. 1973. Voltage-dependent charge movement in skeletal muscle: a possible step in excitation-contraction coupling. *Nature (Lond.)*. 242:244–246.

Schoppa, N. E., K. McCormack, M. A. Tanouye, and F. J. Sigworth. 1992. The size of gating charge in wild-type and mutant Shaker potassium channels. *Science (Wash. DC)*. 255:1712–1715.

Sigg, D., F. Bezanilla, and E. Stefani. 1994. Slowing of deactivation kinetics in *Shaker B* as seen in macropatch recordings of gating and ionic currents. *Biophys. J.* 66:A439. (Abstr.).

Spires, S., and T. Begenisich. 1989. Pharmacological and kinetic analysis of K channel gating currents. *J. Gen. Physiol.* 93:263–283.

Stühmer, W., F. Conti, M. Stocker, O. Pongs, and S. H. Heinemann. 1991. Gating currents of inactivating and non-inactivating potassium channels expressed in *Xenopus* oocytes. *Pflüger Arch.* 418:423–429.

Swenson, R. P., and C. M. Armstrong. 1981. K+ channels close more slowly in the presence of external K+ and Rb+. *Nature (Lond.)*. 291: 427–429.

Taglialatela, M., and E. Stefani. 1993. Gating currents of the cloned delayed-rectifier K^+ channel DRK1. *Proc. Natl. Acad. Sci. USA.* 90:4758–4762.

Taglialatela, M., L. Toro, and E. Stefani. 1992. Novel voltage clamp to record small, fast currents from ion channels expressed in *Xenopus* oocytes. *Biophys. J.* 61:78–82.

Taylor, R. E., and F. Bezanilla. 1983. Sodium and gating current time shifts resulting from changes in initial conditions. *J. Gen. Physiol.* 81:773–784.

Taylor, R. E., J. W. Moore, and K. S. Cole. 1960. Analysis of certain errors in squid axon voltage clamp measurements. *Biophys. J.* 1:160–202.

Tempel, B. L., D. M. Papazian, T. L. Schwarz, Y. L. Jan, and L. Y. Jan. 1987. Sequence of a probable potassium channel component encoded at Shaker locus of Drosophila. *Science (Wash. DC).* 237:770–775.

White, M. M., and F. Bezanilla. 1985. Activation of squid axon K+ channels. *J. Gen. Physiol.* 85:539–554.